Catalysis Science & Technology

Accepted Manuscript

ROYAL SOCIETY OF CHEMISTRY

www.rsc.org/catalysis

Catalysis Science & Technology RSCPublishing

COMMUNICATION

Porous WO_3-Carbon nanofiber: High-Performance and Recyclable Visible-Light Photocatalysis

Cite this: DOI: 10.1039/x0xx00000x

Ahmed Aboueloyoun Taha[a,b*], Fengting Li[b]

Received ooth January 2012,
Accepted ooth January 2012

DOI: 10.1039/x0xx00000x

www.rsc.org/

Template-free porous carbon nanofibers embedded with WO_3 (WO_3-CNF) was prepared by combining electrospinning and carbonization. Ammonium tungstate hydrate was used as a semiconductor precursor and porogen. The generated pores in the CNF matrix formed pathways between the embedded WO_3 and the surface of CNFs, thus, facilitate photo-generated electron transfer.

Introduction

Increasing demand and shortage of clean water sources due to the rapid development of industrialization, population growth and long-term droughts have become an issue worldwide.[1] Photocatalysis proved to be a "green" method that has significant potential for complete decomposition of organic pollutants and deactivation of bacteria in the environment.[2–4] Most of the nanostructured photocatalysts reported to date are TiO_2-based materials, which require UV light for effective photo-catalysis, or it have been constructed in nanoparticle forms, which is very difficult to be separated and recycled.[5–7] Thus, their applied range is severely limited. The materials with one-dimensional (1D) structural, especially for nanofibers, may overcome the above problems.[8] Electrospinning is an attractive approach for generating nanofibers with diameters in the nanometer to micrometer range through the action of a strong electric field imposed on a polymer solution or melt.[9] Besides the high production rate, low-cost and simplicity of the setup, the unique ability of electrospinning is to efficiently form a well-defined 1D membrane with a large surface area and a controlled pore structure.

1D carbon–semiconductor hybrid materials have become a new class of photocatalysts that has attracted considerable attention.[10–12] The composites of carbon and semiconductor photocatalysts possibly offer desirable efficiency for separating electron–hole pairs.[12] Recently various composites of 1D semiconductor/CNF such as TiO_2@carbon embedded by Ag nanoparticles,[13] TiO_2@carbon core/shell nanofiber[8] and ZnO-carbon nanofiber[14] have been synthesized and exhibited high photocatalytic activity. In our previous work,[15] vanadium oxide (VO_x) embedded mesoporous CNF (V-MCNF) was prepared based on one-pot/self-template synthesis strategy, and it showed good photocatalytic activity. It was found that the mesoporous structure creates multi-channelled reaction sites available for mass transfer. These channels provide highly accessible surface areas for the adsorption and photodegradation of contaminants. Moreover, the generated pores in CNFs construct paths between the embedded VO_x and the surface of CNFs, which facilitate electron transfer. We have applied the same synthesis strategy for fabrication of V-MCNF decorated with Fe nanoparticles (co-catalysts) to improve the separation of photogenerated carriers (photogenerated electrons and holes) and the light harvesting efficiencies.[16] The composite displayed superior photocatalytic efficiency due to

photosynergistic effect among the three components of VO_x, carbon and Fe. With its narrow bandgap (Eg =2.6–2.7 eV), WO_3 is a very promising visible-light-active photocatalyst. It has been used in the photocatalytic degradation of organic pollutants,[17] and in the photocatalytic evolution of O_2.[18] However, the photocatalytic activity of pure WO_3 is not satisfactory because of its relatively low conduction-band level (0.5 V vs. NHE). It is generally considered that the conduction band (CB) level of a semiconductor should be more negative than the potential for the single-electron reduction of oxygen ($O_2+e=O^{2-}$ (aq), -0.28 V vs. NHE, or $O_2+H^++e^- = HO_2$ (aq), -0.04 V vs. NHE; NHE = normal hydroge electrode) to allow efficient consumption of photogenerated electrons and subsequent oxidative decomposition of organic compounds. This fact has so far led us to believe that WO_3 is unsuitable for achieving the efficient oxidative decomposition of organic compounds and limited its use as a photocatalysts.[19] Only a few studies have been reported on the oxidative decomposition of organic compounds using WO_3 or its composite-type photocatalysts. Every effort to prevent electron and electron-hole recombination will improve the efficiency of heterogeneous photocatalytic processes and will considerably help to achieve the application of this technique for water and air purification. To improve WO_3 photocatalytic performance, it was modified with Pt,[19,20] Cu,[21] and $CuBi_2O_4$.[22] These materials displayed significantly enhanced photocatalytic activity. Judging from the excellent photocatalyst of WO_3 and the efficient electron transfer property of CNFs, combination of WO_3 and CNFs seems to be ideal for hindering the recombination of electrons and holes and improving the photocatalytic efficiency.

To date, there has been no report on the fabrication of a porous WO_3-CNF photocatalyst with efficient electron-hole separation ability. Herein, we reported a successful attempt for the fabrication WO_3-CNF via simple electrospinning technique and carbonization. The investigation of photocatalytic ability indicated that the WO_3-CNF exhibited excellent photocatalytic activity in the decomposition of different dyes under visible-light irradiation. Furthermore, these WO_3-CNFs could be easily recycled without decrease of the photocatalytic activity due to their one-dimensional nano- structure property.

2. Experimental Section

2.1. Chemicals

Poly(acrylonitrile) (PAN, Mw = 150 000), poly(vinylpyrrolidone) (PVP, Mw = 1 300 000) and ammonium tungstate hydrate (ATH), N,N-Dimethylformamide (DMF), methyl orange (MO), malachite green (MG) and rhodamine B (RB) were purchased from Aldrich Chemical Co. All the above materials were used without further purification.

2.2 Synthesis of WO_3-CNF composite membrane

In a typical one-boat synthesis, 0.05 g ATH was dissolved in 9.0 g DMF at 80 °C for 3 h with vigorous stirring, then 1.0 g PAN was added with continued stirring at the same temperature for 2 h to form homogenous solution. Afterward, the solution was cooled down to the room temperature. The above viscous solution was drawn into a hypodermic syringe for electrospinning. The positive voltage applied to the tip was 16 kV and the distance between the needle tip and the collector was 20 cm. A dense web of membrane fibers was collected on the aluminium foil. To be carbonized, the substrates were first placed in a tube furnace and stabilized in air for 4 h at 250 °C. Then they were subjected to nitrogen gas at 600 °C at a ramp rate 5 °C / minute, and finally they were cooled to the room temperature. The obtained CNF was denoted as WO_3-CNF. For comparison, pure CNF was prepared.

2.3. Characterization instruments and techniques

The scanning electron microscopy (SEM XL30, Philips, Netherlands) and transmission electron microscopy (TEM; high resolution TEM [HRTEM], JEM 2011, JEOL, Japan) were used to characterize the morphology of the products. X-ray diffraction (XRD) measurement was carried out using an X-ray diffractometor (D/MAX-rB, Rigaku, Japan). Ultraviolet-visible spectroscopy (UV-Vis) (UV-2450, Shimadzu, Japan). X-ray photoelectron spectroscopy (XPS) was performed on a RBD upgraded PHI-5000C ESCA system (Perkin Elmer) with Mg Ka radiation (hn=1253.6 eV). Thermogravimetric analysis was conducted on thermogravimetric analyzer (TGA 2050, TA instruments) from 100 to 1050 °C with nitrogen flow rate (5 cm^3/min). Surface areas were calculated by the Brunauer-Emmett-Teller (BET) method, and the pore volume and pore size distributions were calculated using the Barret–Joyner–Halenda (BJH) model.

2.4. Photocatalytic degradation tests.

Photocatalytic decomposition of the dye was carried out in a beaker containing a suspension of 10 mg of the photocatalyst sample in 30 mL dye solution (20 mg/L). Before light was

turned on, the solution was stirred in the dark for 30 minutes to obtain a good dispersion and reach adsorption–desorption equilibrium between the organic molecules and the catalyst surface. The visible light was obtained from 300W tungsten halogen lamp designed surrounded by a quartz jacket for cooling, and the beaker was placed 5 cm away from the visible-light lamp. At a given interval of illumination, the samples of the reaction solution were taken out and analyzed by a Shimadzu UV/VIS (1700) spectrophotometer. To evaluate the reusability of the catalyst several photocatalytic degradation runs of MO-dye were completed under visible light. After the first run, the catalyst was separated and used immediately for further cycles without any treatment.

3. Result and discussion

Figs. 1A and B present the SEM images of CNF and WO_3-CNF. Fig. 1A shows randomly oriented CNFs having a smooth and uniform surface. The diameter of the pure CNF ranged from 250 nm to 300 nm. The SEM image of WO_3-CNF shown in Fig. 1B indicates that the nanofiber became curvy and the fibers diameter was slightly increased (350 nm). The increased diameter is surely from the high viscosity due to the addition of ATH into the PAN polymer solution. However, the SEM image of WO_3-CNF revealed a smooth surface of the fibers without the mass of tungsten particles. The absence of tungsten particles suggests that WO_3 was successfully incorporated into the carbon-fiber matrix.

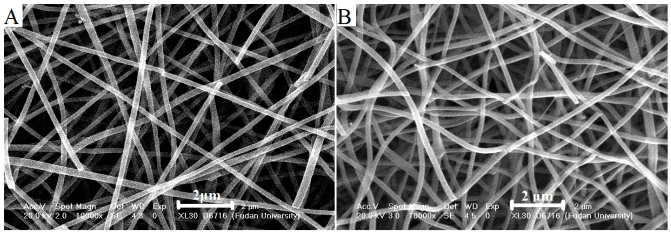

Fig. 1. (A) SEM image of CNF and (B) SEM image of WO3-CNF.

Figs. 2A and B present the TEM and HRTEM images of CNF and WO_3-CNF, respectively. The fiber exhibited a rough and uniform surface, which is consistent with the SEM observation. From the HRTEM images, we can see white worm-like structures appeared on the surface of carbon fiber. These structures were generated during the carbonization of WO_3-CNF samples due to the decomposition of ATH, which previously grew in the black CNF. The decomposition of ATH contributed to pore generation, which connected the inside WO_3 to the surface of CNF. We have reported similar observation when the ammonium metavanadate was incorporated in the CNF.[15] Fig. 2C presenting the thermogravimetric analysis (TGA) curve of WO_3-CNF sample. It shows that about 25 wt% of the sample was lost at 330 °C due to the decomposition of the organic components. At 410 °C, ATH started to produce the intermediate compounds species to form WO_3. It suggests that ATH was acted as the build-in template.

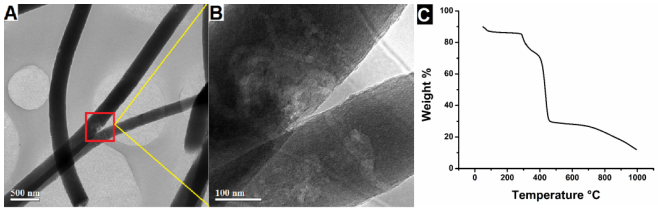

Fig. 2. (A) TEM image of WO_3-CNF, (B) HRTEM image of WO_3-CNF and (C) TGA data of WO_3-CNF.

Fig. 3 shows the XRD patterns of CNF and WO_3-CNF. The XRD patterns of the CNF shows a graphite diffraction peaks at 25° and 43° corresponding to (002) and (101) planes, indicate the presence of graphite-like carbon [Fig. 3A (a)]. However, the broad peaks and a complete absence of higher order peaks in the XRD patterns suggest low graphitization and disordered amorphous structure for the prepared materials.[24] The XRD pattern of WO_3-CNF [Fig. 3A (b)] showed that no peaks attributed to tungsten oxides were detected. This indicates that tungsten oxides were successfully incorporated into the crystal lattice of CNFs or they were too little to be completely detected by XRD. However, the intensity of graphitic CNF peaks of WO_3-CNF became weaker because of the destruction of graphitic layers while the decomposition of ATH by carbonization. Fig. 3B represents the profound effect of the WO_3 content in UV–vis absorption spectrum of the WO_3-CNF catalyst. Compared to standard WO_3, the as-prepared catalyst sample retains a substantial amount of the visible light absorption (λ> 400 nm). The reason for the strong absorption of visible light could be attributed to two reasons: one was from the carbon itself which could absorb visible light; the other was a joint electronic system formed between WO_3 and carbon, which gave rise in synergistic properties.

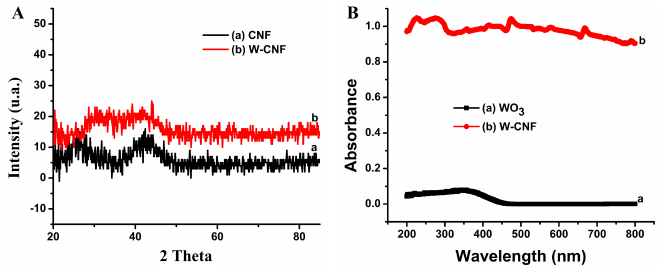

Fig. 3. (A) XRD patterns of the samples of CNF and WO_3-CNF, (B) UV/Vis diffuse-reflectance spectra of the sample of WO_3 and WO_3-CNF.

To investigate the elemental contents on the surface of samples, EDS data are presented in Table 1 (for EDS element analysis see ESI† Fig. 1S). In the case of CNF, it consisted of showing elements content of 84.1 % and 13.05 % for carbon and oxygen, respectively. In the case of WO_3-CNF sample, tungsten element was about 4.99 % and oxygen was 23.66 %. The carbon yield was decreased in the WO_3-CNF sample, because of the decomposition of ATH and generating the pores in the CNF. On the contrary, the oxygen content was increased due to the increase of the oxygen attached with the tungsten. Moreover, the XPS detected an approximately 3 % of nitrogen in both samples. The existence of the nitrogen is due to the thermal treatment of the samples under N_2. The BET surface area demonstrates that WO_3-CNF has greater surface area (445 $m^2 g^{-1}$) than the CNF (218 $m^2 g^{-1}$). And, the average pore size and volume of WO_3-CNF were larger than that of CNF. The higher surface area of WO_3-CNF is because of the generated pores by the decomposition of ATH during the carbonization as discussed previously.

Table 1. Physical and chemical properties of the prepared composite.

Sample	Element composition on surface (%)				Average pore size (nm)	Average pore volume ($cm^3 g^{-1}$)	BET ($m^2 g^{-1}$)
	C	O	W	N			
CNF	84.10	13.05	-	2.8	1.04	0.02	218.98
WO_3-CNF	56.50	23.66	4.98	2.9	2.03	0.12	445.46

The nitrogen adsorption–desorption isotherms for WO_3-CNF shown in ESI† Fig. 2S(A) is a typical type I behavior representing the microporous adsorption. However, the pore size distribution presented in ESI† Fig. 2S(B) clearly confirmed the existence of bimodal pores with detectable sizes of 1.7 and 1.9 nm to 2.3 nm. As we previously reported,[15] pure CNF exhibited micropores at a mean value of 1.7 nm, which generated during the carbonization process. Thus, the generated pores in WO_3-CNF sample with the size of 1.9-2.3 nm is due to the decomposition of ATH and its porogen role.

Since the WO_3-CNF had remarkable light absorption in the visible region, and high surface area, we assumed that it present high photo-chemical activity in the visible-light region. Therefore, we carried out experiments of the photocatalytic degradation of MB as a test reaction. In the experiments, commercial WO_3 used as a photocatalytic reference and the degradation efficiency of the as-prepared samples was defined. The absorption spectra of MB aqueous solution showed the change of its concentration. The MB concentration (%) after various intervals of time could be estimated using the following equation:

$$\% \text{ MO concentration} = (C/C_0)\times 100 \qquad (1)$$

where C_0 is the initial MO absorbance and C is the absorbance obtained after various intervals of time. As observed in Fig. 4A, the control experiments were performed under different conditions: (1) in the presence of photocatalysts but in the dark and (2) with visible-light irradiation but in the absence of the photocatalysts. These results showed that the adsorption-desorption equilibrium of MB in the dark was established within 30 minutes. And, there was no significant degradation of MB after 1 h in the absence of photocatalysts. Fig. 4B shows the degradation curves of MB over commercial WO_3, CNF and WO_3-CNF under the visible-light irradiation. As it can be seen, negligible degradation efficiency was observed with adding WO_3 or CNF for 10 minutes. Notably, the degradation efficiency of MB was 100 % over WO_3-CNF sample only after 5 minutes. The stability of the photocatalyst is very important for the application in environmental technology. Therefor, three cycles experiment of MB degradation over the WO_3-CNF was carried out. As shown in Fig. 4C, the photocatalytic degradation efficiency of the novel material under visible-light irradiation was maintained in high efficiency. More importantly, it was indicated that the WO_3-CNF with superior photocatalyst activity could be easily separated and recovered by sedimentation due to the 1D structure property, which would greatly promote its practical application to eliminate the organic pollutants from wastewater. Furthermore, in order to confirm the photodegradation efficiency and application feasibility of WO_3-CNF, it was examined with MG and MO dyes. As shown in Fig. 4D, the WO_3-CNF exhibited 100% decomposition of

MG and MO after exposure to the visible-light for 6 and 10 minutes, respectively.

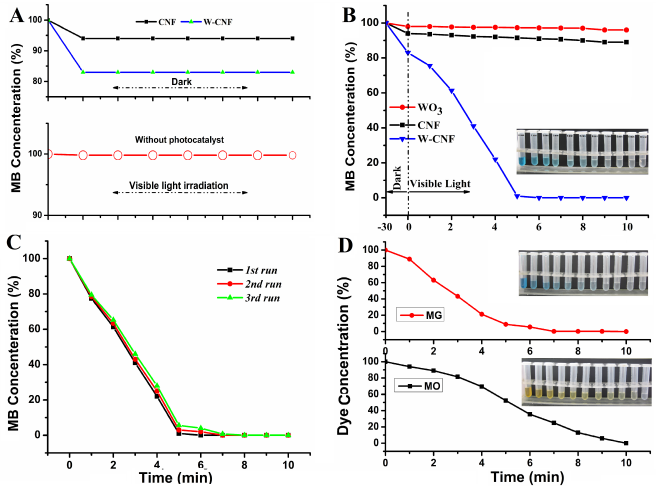

Fig. 4. (A) Degradation profiles of MB in the presence of the CNF and WO_3-CNF photocatalysts but in the dark and with visible light irradiation but in the absence of photocatalysts. (B) Degradation profiles of MB over different samples (30 ml of aqueous dye, 20 mg/L, and 10 mg of the photocatalyst). (C) Photocatalytic activity of the sample WO_3-CNF for MB degradation with three times of cycling uses. (D) Degradation profiles of MG and MO over WO_3-CNF (30 ml of aqueous dye, 20 mg/L, and 10 mg of the photocatalyst).

To further study the chemical and bonding environment of the components of the prepared WO_3-CNF composite including carbon phase and tungsten oxide. X-ray photoelectron spectroscopy (XPS) was applied. Fig. 5A shows the complete spectra over the range of 0-1000 eV. This overview spectrum demonstrates that C, O, W, and N atoms were present in the sample. Fig. 5B shows the high resolution XPS spectrum of the C1s region at approximately 285 eV. The binding energy with a peak at 284.4 eV was attributed to sp^2-hybridization bonding structures of C atoms bonded to N atoms (sp^2 C═N).[23] The peaks at 286.8 and 287.9 eV were characteristic of the oxygen-bound species C=O and C–O,[24,25] respectively. The last small broad band at 290–291 eV was assigned to the shakeup π–π* satellite, which is a common feature of graphitic carbon in XPS spectra.[26] Fig. 5C shows the high resolution XPS spectrum of W 4f. According to the W4f peaks, two strong peaks at 35.3 eV and 38.0 eV corresponding to W 6 + and two medium peaks at 36 eV and 36.7 eV may be resulted from the emission of $W4f_{5/2}$ and $W4f_{7/2}$ core levels from the atoms in a valence state of 5+.[27,28] The high resolution XPS spectrum of N 1s (Fig. 5D) indicates the existence heterocyclic N molecules such as (1): pyridinic N (398.3 eV), (2): pyrrolic or pyridine N (400.1 eV), (3): quaternary N (401.3 eV), and (4): oxidized N (402.6 eV).[29,30] Indeed the incorporation of nitrogen leads to a beneficial effect in view of the intended photoelectron-chemical applications.[31] However, further investigations are needed to understand the role of N in the photocatalysis mechanism of WO_3-CNF.

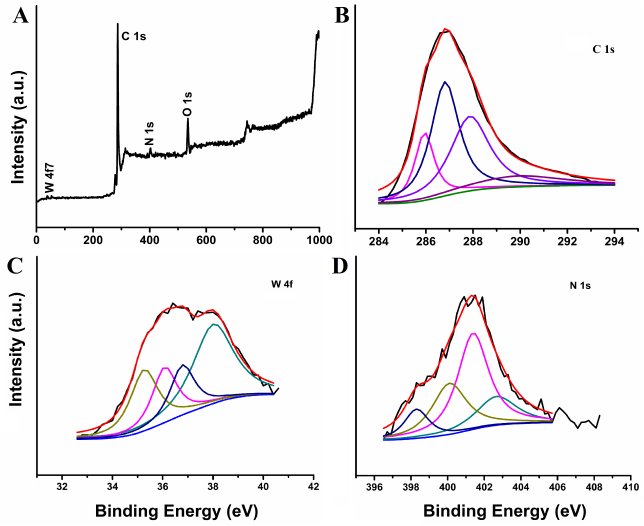

Fig. 5. (A) XPS fully scanned spectra of the WO_3-CNF, (B) XPS spectra of C1s for the WO_3-CNF, (C) XPS spectra of W 4f for the WO_3-CNF and (D) XPS spectra of N 1s for the WO_3-CNF.

Conclusions

In summary, porous WO3-CNF photocatalyst was prepared based on self-template strategy by simple electrospinning technique and carbonization. The investigation of photocatalytic ability indicated that the WO3-CNF exhibited excellent photocatalytic activity in the decomposition of different dyes under visible-light irradiation. Furthermore, these WO3-CNF could be easily recycled without decrease of the photocatalytic activity due to their one-dimensional nano-structure property. The present results indicate that incorporating semiconductors in CNF is an effective strategy for the development of highly efficient and durable visible-light driven photocatalysts based on a simple synthesis method.

Notes and references

[a] College of Environmental Science and Engineering, UNEP Tongji Institute of Environment for Sustainable Development, State Key Laboratory of Pollution Control and Resource Reuse Study, Tongji

University, Siping Rd 1239, Shanghai, 200092, China. Fax: +86-21-65985059; Tel: +86-21-65983121; Email: taha@tongji.edu.cn, ahmadoyoun@gmail.com.

[b] Soils, Water and Environment Research Institute (SWERI), Agricultural Research Center (ARC), Giza 12112, Egypt.

† Electronic Supplementary Information (ESI) available: [DES analysis of CNF and WO_3-CNF, N_2 adsorption–desorption isotherms and the corresponding pore size distribution of the sample of WO_3-MCNF composite membrane.]. See DOI: 10.1039/c000000x/

1. M. N. Chong, B. Jin, C. W. K. Chow, and C. Saint, *Water Res.*, 2010, **44**, 2997–3027.
2. T. Arai, M. Horiguchi, M. Yanagida, T. Gunji, H. Sugihara, and K. Sayama, *Chem. Commun. (Camb).*, 2008, 5565–5567.
3. H. Zeng, W. Cai, P. Liu, X. Xu, H. Zhou, C. Klingshirn, and H. Kalt, *ACS Nano*, 2008, **2**, 1661–1670.
4. X. Zhou, C. Hu, X. Hu, T. Peng, and J. Qu, *J. Phys. Chem. C*, 2010, 2746–2750.
5. J. Yu, G. Dai, and B. Huang, *J. Appl. Chem. C*, 2009, **113**, 16394–16401.
6. L. Kuai, B. Geng, X. Chen, Y. Zhao, and Y. Luo, *Langmuir*, 2010, **26**, 18723–7.
7. G. Xi, B. Yue, J. Cao, and J. Ye, *Chemistry*, 2011, **17**, 5145–54.
8. P. Zhang, C. Shao, Z. Zhang, M. Zhang, J. Mu, Z. Guo, and Y. Liu, *Nanoscale*, 2011, **3**, 2943–9.
9. Y. Wu, W. Jia, Q. An, Y. Liu, J. Chen, and G. Li, *Nanotechnology*, 2009, **20**, 245101.
10. W. Guo, F. Zhang, C. Lin, and Z. L. Wang, *Adv. Mater.*, 2012, **24**, 4761–4.
11. L. Liao, M. Zheng, Z. Zhang, B. Yan, X. Chang, G. Ji, Z. Shen, T. Wu, J. Cao, and J. Zhang, *Carbon N. Y.*, 2009, **47**, 1841–1845.
12. Q. Xiang, J. Yu, and M. Jaroniec, *Chem. Soc. Rev.*, 2012, **41**, 782–96.
13. P. Zhang, C. Shao, Z. Zhang, M. Zhang, J. Mu, Z. Guo, Y. Sun, and Y. Liu, *J. Mater. Chem.*, 2011, **21**, 17746.
14. J. Mu, C. Shao, Z. Guo, Z. Zhang, M. Zhang, P. Zhang, B. Chen, and Y. Liu, *ACS Appl. Mater. Interfaces*, 2011, **3**, 590–596.
15. A. A. Taha, A. a. Hriez, H. Wang, Y. Wu, and F. Li, *RSC Adv.*, 2014, **4**, 5901.
16. A. A. Taha, A. a. Hriez, Y. Wu, H. Wang, and F. Li, *J. Colloid Interface Sci.*, 2014, **417**, 199–205.
17. D. Chen, L. Gao, A. Yasumori, K. Kuroda, and Y. Sugahara, *Small*, 2008, **4**, 1813–22.
18. D. Chen and J. Ye, *Adv. Funct. Mater.*, 2008, **18**, 1922–1928.
19. R. Abe, H. Takami, N. Murakami, and B. Ohtani, *J. Am. Chem. Soc.*, 2008, **130**, 7780–1.
20. Z.-G. Zhao and M. Miyauchi, *Angew. Chem. Int. Ed. Engl.*, 2008, **47**, 7051–5.
21. H. Irie, S. Miura, K. Kamiya, and K. Hashimoto, *Chem. Phys. Lett.*, 2008, **457**, 202–205.
22. T. Arai, M. Yanagida, Y. Konishi, Y. Iwasaki, H. Sugihara, and K. Sayama, *J. Phys. Chem. Lett.*, 2007, 7574–7577.
23. J. Shalini, K. J. Sankaran, C.-L. Dong, C.-Y. Lee, N.-H. Tai, and I.-N. Lin, *Nanoscale*, 2013, **5**, 1159–67.
24. F. Xia, X. Hu, Y. Sun, W. Luo, and Y. Huang, *Nanoscale*, 2012, **4**, 4707–11.
25. O. Jankovský, P. Šimek, D. Sedmidubský, S. Matějková, Z. Janoušek, F. Šembera, M. Pumera, and Z. Sofer, *RSC Adv.*, 2014, **4**, 1378.
26. J. J. Lee Jun Seop, Kwon Oh Seok, Park Seon Joo, Park Eun Yu, You Sun Ah, Yoon Hyeonseok, *ACS Nano*, 2011, **5**, 7992–8001.
27. X. Cui, H. Zhang, X. Dong, H. Chen, L. Zhang, L. Guo, and J. Shi, *J. Mater. Chem.*, 2008, **18**, 3575.
28. C. Guo, S. Yin, Q. Dong, and T. Sato, *CrystEngComm*, 2012, **14**, 7727.
29. H. R. Byon, J. Suntivich, J. Crumlin, and Y. Shao-horn, 2011, 21437–21445.
30. N. Dong, S. Jeong, G. Kim, I. Nam, H. Jin, P. Kim, and J. Yi, *Electrochim. Acta*, 2012, **78**, 340–346.
31. Y.-C. Nah, I. Paramasivam, R. Hahn, N. K. Shrestha, and P. Schmuki, *Nanotechnology*, 2010, **21**, 105704.